

This discussion paper is/has been under review for the journal *Atmospheric Chemistry and Physics (ACP)*. Please refer to the corresponding final paper in *ACP* if available.

Intercomparison of integrated IASI and AATSR calibrated radiances

S. M. Illingworth, J. J. Remedios, and R. J. Parker

EOS, Space Research Centre, Department of Physics and Astronomy, University of Leicester, Leicester, LE1 7RH, UK

Received: 24 February 2009 – Accepted: 12 March 2009 – Published: 27 March 2009

Correspondence to: S. Illingworth (smi3@le.ac.uk)

Published by Copernicus Publications on behalf of the European Geosciences Union.

Title Page

Abstract

Introduction

Conclusions

References

Tables

Figures

◀

▶

◀

▶

Back

Close

Full Screen / Esc

Printer-friendly Version

Interactive Discussion



Abstract

The mission objectives of the Infrared Atmospheric Sounding Interferometer (IASI) are driven by the needs of the Numerical Weather Prediction (NWP) and climate monitoring communities. These objectives rely upon the IASI instrument being able to measure top of atmosphere radiances accurately. This paper presents a technique and results for the validation of the radiometric calibration of radiances for IASI, using a cross-calibration with the Advanced Along Track Scanning Radiometer (AATSR). The AATSR is able to measure Brightness Temperature (BT) to an accuracy of 30 mK, and by applying the AATSR spectral filter function to the IASI measured radiances we are able to compare AATSR and IASI Brightness Temperatures. By choosing coincidental data points that are over the sea and in clear sky conditions, a threshold of homogeneity is derived. It is found that in these homogenous conditions, the IASI BTs agree with those measured by the AATSR to within 0.5 K, with a precision of order 0.04 K. These results indicate that IASI is likely to be meeting its target objective of 0.5 K accuracy. It is believed that a refinement of the AATSR spectral filter function will hopefully permit a tighter error constraint on the quality of the IASI data and hence further assessment of the climate quality of the radiances.

1 Introduction

The Infrared Atmospheric Sounding Interferometer (IASI) is a nadir sounding Fourier transform spectrometer flying operationally on the MetOp-A satellite, and which will operate also on the two subsequent satellites of the MetOp programme; the resulting record of spectrally resolved radiances should span at least 15 years. Geophysically, the accuracy of these radiances is very important for a number of reasons. Firstly, these radiances have a direct impact on the derivation of air and surface temperature, humidity, and composition profiles for which IASI is already beginning to deliver interesting results. This atmospheric composition data will be significant for climate, as

Title Page

Abstract

Introduction

Conclusions

References

Tables

Figures



Back

Close

Full Screen / Esc

Printer-friendly Version

Interactive Discussion



well as numerical weather prediction applications. Secondly, the spectrally resolved radiances can be used to study directly the long-term radiance change over decades (Harries et al., 2001), or to directly test radiation schemes within General Circulation Models (GCMs) (Huang et al., 2007). Finally, a long-term series of calibrated radiances can and will be used for the direct testing of the outputs of GCMs (e.g., Haskins et al., 1999; Brindley et al., 1999); calibrated radiances are effectively to be considered a geophysical product in themselves, as they represent Top of the Atmosphere (TOA) radiation at the appropriate wavelengths of the data.

There are two important consequences of developing climate time series of either radiance itself or derived geophysical products. Firstly, it is important to intercompare well-calibrated, long-term instruments, where possible, thus providing independent verification of radiances. Secondly, it is a valuable and necessary exercise to undertake such tests as part of a long-term testing strategy which can evaluate trends in instrument calibration. This paper is directed towards the development of a methodology for the former, and the provision of first results for this aspect for the IASI instrument. The intercomparison studied here is between the calibrated and geophysically located, Level 1, TOA radiances for the IASI and the Advanced Along Track Scanning Radiometer (AATSR) on ENVISAT.

This paper is organised as follows: the description of the IASI and AATSR instruments used in the cross-calibration is provided in Sect. 2. Section 3 describes the cross-calibration technique used to radiometrically calibrate the IASI instrument and presents the results of this process. Section 4 concludes this study with some perspectives on this work, discussing what the results of the cross-calibration imply for the radiometric accuracy of the IASI instrument.

[Title Page](#)[Abstract](#)[Introduction](#)[Conclusions](#)[References](#)[Tables](#)[Figures](#)[I◀](#)[▶I](#)[◀](#)[▶](#)[Back](#)[Close](#)[Full Screen / Esc](#)[Printer-friendly Version](#)[Interactive Discussion](#)

2 The instruments

2.1 IASI

The IASI instrument (Phulpin et al., 2007; Clerbaux et al., 2007; CNES, 2008) is a nadir viewing Fourier transform spectrometer. The MetOp Equator crossing time is 09:30 Local Solar Time (LST) in a polar sun-synchronous orbit. A swath (120 views) is achieved in 8 s, allowing global coverage twice a day, and each IASI pixel has a footprint of 12 km diameter at nadir. The instrument covers the spectral range between 645–2760 cm^{-1} (15.5–3.6 μm), but in three overlapping bands: 645–1240 cm^{-1} (5.1–3.6 μm), 1200–2000 cm^{-1} (8.3–5.0 μm), and 1960–2760 cm^{-1} (15.5–8.3 μm). The instrument has a maximum optical path difference of ± 2 cm giving a nominal apodised spectral resolution of 0.5 cm^{-1} , with a spectral sampling of 0.25 cm^{-1} (Blumstein et al., 2004).

The IASI instrument is designed to be calibrated to an absolute brightness temperature of at least 1 K (objective 0.5 K). It is radiometrically calibrated using views of an internal hot blackbody, whose temperature can be modified and is carefully monitored (typically 293 K), a cold blackbody held at a temperature below 100 K (typically 95 K), and views of deep space. In addition, a non-linearity correction is performed for the Band 1 (B1) detector which is photoconductive. Details are given in Blumstein et al. (2004), which notes that accuracies of better than 0.25 K are shown by ground calibration, and that effects include the non-linearity of B1, as well as small deviations from perfect emissivity of the internal blackbodies and the ground calibration reference blackbodies.

The IASI data used in this paper are the Level 1C data which consist of geolocated and apodised spectra. The data used in this paper are the operationally produced version 2.0 data set.

Title Page

Abstract

Introduction

Conclusions

References

Tables

Figures

◀

▶

◀

▶

Back

Close

Full Screen / Esc

Printer-friendly Version

Interactive Discussion



2.2 AATSR

The AATSR, on the Environmental Satellite (Envisat), is used here as the reference inter-comparison instrument; the Envisat equator crossing time is 10:00 LST. The AATSR is a dual-view, scanning radiometer with a 1 km^2 footprint for the nadir view at the sub-satellite point. It has seven channels, including three thermal channels: the two split-window channels at 11 and $12 \mu\text{m}$, and a third infrared channel at $3.7 \mu\text{m}$, which is only used at night as it is contaminated by reflected solar radiation during the day. The filter functions for the 11 and $12 \mu\text{m}$ channels are shown in Fig. 2. More details about the AATSR instrument are given in Llewellyn-Jones et al. (2001); Smith et al. (2001); ESA (2008).

The AATSR instrument uses an exceptionally stable on-board calibration system for its infrared channels, resulting in a high intrinsic radiometric sensitivity and accuracy. Two targets (“hot” and “cold” at approximately 301 K and 263 K respectively) are viewed every scan for calibration, and the detectors are cooled to 80 K by a Stirling Cycle cooler to ensure that the radiometric noise of these channels at 270 K is $<0.05 \text{ K}$. The AATSR is radiometrically calibrated to a high accuracy; pre-launch calibration using high-accuracy external black bodies indicated that the AATSR BTs were within 30 mK of target temperatures for the 11 and $12 \mu\text{m}$ channels (Smith et al., 2001). The heritage of the instrument design is well proven since AATSR is the third instrument (for results for radiometric design and accuracy of the earlier ATSR-1 and ATSR-2 instruments see e.g., Mutlow et al., 1994) founded on well-designed black bodies for radiometers (Mason et al., 1996).

In this paper, only the nadir-view AATSR data in the 11 and $12 \mu\text{m}$ channels are used as the channel at $3.7 \mu\text{m}$ does not provide both day and night data, and also the full AATSR bandpass does not fall completely within the IASI band pass. The AATSR Level 1B V2.0 data were obtained from the NEODC UK Archive of AATSR data.

Title Page

Abstract

Introduction

Conclusions

References

Tables

Figures

◀

▶

◀

▶

Back

Close

Full Screen / Esc

Printer-friendly Version

Interactive Discussion



3 Cross calibration of IASI and AATSR

3.1 Overview of concept

Sensor radiometric calibration involves well-known processes such as pre-flight calibration, on-board calibration and, in the case of optical sensors, vicarious calibration against well-known targets; these approaches are well documented (e.g, Dingirard and Slater, 1999). For the thermal infra-red, pre-flight and on-board calibration are also standard. However the cross-calibration of satellite instruments against “well-known” targets has proved to be more of an issue, because scene temperature and atmospheric state variability are critical parameters, and a mismatch in time (for example), can cause significant differences in observed TOA radiances. Further issues arise because of differing spectral filter functions and differing views of the instruments to be compared. Some of these issues have been examined, for example, by Merchant et al. (2003), who developed radiance correction factors for the Visible Infrared Spin-Scan radiometer on-board the Japanese Geostationary Meteorological Satellite (GMS-5), using equivalent data from the ATSR-2 instrument.

The advent of spectrometers such as IASI and the Atmospheric Infrared Sounder (AIRS) has provided more scope for cross-calibration against radiometer TOA data, since the radiometer may be more easily compared using integration of the measured TOA *spectral radiances* of IASI/AIRS for co-located fields-of-view. A particularly attractive aspect of this comparison is that the integration can utilise exactly the assumed spectral passbands of the radiometers, without the need for interpolation or radiative transfer modelling (see Sect. 3.2 for exact conditions). Geophysically, it enables TOA radiance measurements from radiometers, usually at higher spatial resolution, to be linked radiometrically to TOA spectrally resolved radiance measurements at lower spatial resolutions. This provides a nice match of characteristics for testing climate models, especially if such a combined system of TOA radiance measurements can form a long time series.

Preliminary work for such spectrometer-radiometer intercomparisons has been per-

Title Page

Abstract

Introduction

Conclusions

References

Tables

Figures



Back

Close

Full Screen / Esc

Printer-friendly Version

Interactive Discussion



formed, (e.g., Qu et al., 2005; Wang and Cao, 2007), but so far such comparisons have not used an instrument like the AATSR, which has been designed for high radiometric accuracy. In this study we focus intentionally on comparing the IASI and AATSR instruments, for which we have a good knowledge of radiance calibration on the ground, but wish to intercompare the performance of the systems in space. In particular, we examine how well such a comparison can be carried out by focussing on the intercomparison for surfaces with well understood characteristics, in a manner analogous to the vicarious calibration of visible sensors.

3.2 Cross-calibration match-ups

Thermal infra-red TOA radiances vary strongly with wavelength, surface temperature and emissivity, atmosphere temperatures, atmosphere composition (particularly humidity), and clouds. Therefore, for the most accurate intercomparison of radiances, it is ideal to consider surfaces of largely uniform emissivity, close matches in time and space, and similar view angles. These factors are now considered in turn.

The AATSR thermal channels at 11 μm and 12 μm are designed to be able to determine surface temperature, particularly over the oceans, with very good accuracy. For the present purpose, scenes with both a uniform surface emissivity and small changes of surface temperature with time are ideal. Oceans satisfy both criteria in general (rather than land), and thick clouds may at least satisfy the first criterion but quite possibly the second. Therefore, this paper focusses firstly on clear sky ocean scenes and subsequently considers results for cloudy scenes (see Sect. 3.3 for the classification system) over the ocean. Issues with the AATSR cloud flagging over land preclude use of these data for accurate radiometric calibration work.

In order for a very good cross-calibration to be performed, the measured BTs for both instruments need ideally to be taken from the same geographic (latitude and longitude) location (co-located view), and measured at similar times. The AATSR achieves global coverage approximately once every three days, with a repeat cycle of 35 days (ESA, 2008). In comparison IASI achieves twice daily coverage with a 29 day repeat cycle

Title Page

Abstract

Introduction

Conclusions

References

Tables

Figures



Back

Close

Full Screen / Esc

Printer-friendly Version

Interactive Discussion



(Camy-Peyret and Eyre, 1998). As the two instruments have equator crossing times that differ by only half an hour, there will be some measurements where the two orbits become coincident at approximately the same time. Fig. 1 shows that on 01/09/2007 the views of the two instruments coincided on both a spatial and temporal scale. The red box indicates an example area in which this occurs. All the results in this study are taken from this day but utilising all orbits as opposed to the single orbit match-up shown on the plot.

The match-ups were further constrained by two factors. First, only the sub-satellite IASI nadir views were used, and then the AATSR nadir-view data found that matched in space with these observations (see below). The match-ups were then further limited to only those occurring within 20 min of each other, in order to limit the possibility that the cloud scene will have changed between the IASI and AATSR views of the same scene; this is conservative compared to the mean time difference of 24 min in the work of Merchant et al. (2003). Since thermal emission at $11\ \mu\text{m}$ and $12\ \mu\text{m}$ does not substantially change its characteristics diurnally, both day and night data are used in the comparison.

In nadir mode, the horizontal resolution of the AATSR instrument is $1\ \text{km}^2$, whilst the pixel size of the IASI instrument at the sub-satellite point is approximately $113\ \text{km}^2$ (radius of 6 km). Hence within the criteria of very good coincidence with the sub-satellite IASI sub-satellite nadir view, there should be over 100 AATSR measurements within each IASI pixel.

3.3 Radiance comparisons

Having defined the match-ups between the IASI and AATSR data sets, the IASI spectrally resolved TOA radiances were integrated to “AATSR-like” radiances, and then converted to radiometric brightness temperatures (BTs) which is the equivalent form of the AATSR TOA radiances. The AATSR spectral filter functions for the channels $11\ \mu\text{m}$ and $12\ \mu\text{m}$ are shown in Fig. 2. For the selected regions, the mean and standard deviation of the AATSR BTs within each IASI pixel were then calculated, and also the

[Title Page](#)[Abstract](#)[Introduction](#)[Conclusions](#)[References](#)[Tables](#)[Figures](#)[I◀](#)[▶I](#)[◀](#)[▶](#)[Back](#)[Close](#)[Full Screen / Esc](#)[Printer-friendly Version](#)[Interactive Discussion](#)

match-ups flagged for cloud and sea/land. The standard deviations are subsequently used to illustrate the homogeneity of the scenes and for the cloud scenes to perform a cross-calibration consistent with the clear sky comparisons.

Further classification was performed using the flags associated with the AATSR data flags for land and cloud, since the AATSR instrument has the higher spatial resolution. The AATSR contains a detailed cloud-filtering system which labels each AATSR pixel as being either “clear sky” or “cloudy”; the cloud processor is described in Zavody et al. (2000). The cloud and land filters of the AATSR data set within each IASI coincident view were used to separate the match-ups into different sub-groups which could be further analysed. IASI pixels containing only “land” AATSR pixels were assumed to have been taken over the land, whilst those containing only “sea” AATSR pixels were assumed to be have been taken over the sea; land pixels were not subsequently used in the analysis. Any IASI pixels which were deemed as being over both land and sea (such as a coastline) were also discarded, as they were too few in number to draw any significant statistical conclusions from. The IASI measurements over ocean were then separated into three further groups: data that was cloud-free (contained only clear sky AATSR pixels), data that was fully-cloudy (contained only cloudy AATSR pixels), and data that was fractionally cloudy (contained both clear sky and cloudy AATSR pixels). Thus each match-up between IASI was labelled with the AATSR-like IASI BT, the mean AATSR BT in the IASI pixel and the standard deviation of the AATSR BTs, the sea/land flag and a cloud group flag. Recall that comparisons of measurements that are made over the land are not dealt with in this paper, as even though the temporal agreement between the two datasets is good it is not absolute and significant temperature changes can occur over 20 min. The sea represents a far more homogenous surface than the land, with radiometric observations unlikely to have changed during the time between the IASI and AATSR measurements being taken. Cloud free conditions over the sea are most likely to allow for the greatest homogeneity of the scene.

Title Page

Abstract

Introduction

Conclusions

References

Tables

Figures



Back

Close

Full Screen / Esc

Printer-friendly Version

Interactive Discussion



3.4 Cross-calibration results

Results for the differences between IASI equivalent BTs and the AATSR mean BTs are shown in Fig. 3, for each classification (clear sky, cloudy etc.) and for the 11 μm channel as a function of the AATSR BT standard deviation within each IASI pixel. The clear sky data show very small deviations (less than 0.16 K) with much larger variations for the pixels containing fractional or cloudy pixels. The fractional and completely cloudy data have very large standard deviations, as well as mean differences, as expected. Hence we consider first the clear sky data.

The results for the cross-calibration over the 11 μm and 12 μm spectral domains, for measurements taken over the sea and in cloud free conditions, are shown in Fig. 4. This plot shows that there is a very strong correlation between the AATSR and IASI BTs, in both the 11 μm and 12 μm spectral regions, over a temperature range of just greater than 10 K. It also shows that the IASI instrument underestimates the BTs, compared to those measured by the AATSR instrument. This discrepancy is indistinguishable between channels, within the errors for the 11 μm spectral region, a mean IASI-AATSR BT difference of -0.46 K (error of 0.03 K on the mean; 31 points) is observed, compared to -0.38 K in the 12 μm region (error of 0.04 K, 31 points). In both spectral regions, the mean BT difference is less than 0.5 K, with a small standard deviation, indicating that the IASI instrument is in agreement with the AATSR instrument to at least this level, in cloud-free scenes. Therefore the indication would be that IASI is likely to be meeting its target objective over ocean clear sky conditions.

The clear sky comparisons for this day are limited in their temperature range. However, the real criterion for conducting a comparison is a uniform scene rather than requiring the scene to be free of clouds. Therefore, the comparisons were extended to include all pixels with AATSR BT standard deviations less than 0.16 K (the clear sky maximum standard deviation). Figure 5 shows the resulting relationship between the IASI and AATSR BTs for all such data points. It is immediately clear that the temperature range is now larger with a lower temperature bound at 260 K. The correlation

Title Page

Abstract

Introduction

Conclusions

References

Tables

Figures



Back

Close

Full Screen / Esc

Printer-friendly Version

Interactive Discussion



IASI Validation

S. Illingworth et al.

[Title Page](#)[Abstract](#)[Introduction](#)[Conclusions](#)[References](#)[Tables](#)[Figures](#)[◀](#)[▶](#)[◀](#)[▶](#)[Back](#)[Close](#)[Full Screen / Esc](#)[Printer-friendly Version](#)[Interactive Discussion](#)

coefficient improves but this is as expected and is simply a consequence of the increase in temperature range. The mean differences between IASI equivalent BTs and AATSR mean BTs are now -0.49 K for the $11\ \mu\text{m}$ channel (error on the mean of 0.04 K; 87 points) and -0.39 K for the $12\ \mu\text{m}$ channel (error on the mean of 0.04 K; 90 points).

5 There is now a marginally significant difference between the comparison in the two channels. Overall though, the agreement between the two instruments remains good to at least 0.5 K over a wide range of temperatures.

Based on the assumption that the AATSR is intrinsically radiometrically calibrated to an accuracy of 30 mK, these results would seem to indicate that the IASI instrument is itself able to measure BTs to an accuracy of better than 0.5 K. However, the comparison does rely on knowledge of the AATSR spectral filter functions. Currently there are some uncertainties in the exact knowledge of these filter functions to at least the 0.2 K level. Therefore, the current results are best viewed as indicating an absolute comparison of the two instruments to probably the 0.5 K level, and consequently an absolute calibration uncertainty for IASI of 0.5 K.

4 Conclusions

Based on the cross-calibration results in this study, integrated IASI radiances agree very well with AATSR BTs at $11\ \mu\text{m}$ and $12\ \mu\text{m}$, and indicate that IASI is likely to be meeting its target objective of 0.5 K accuracy. The estimated IASI equivalent BTs are lower than the AATSR BTs, and this appears to be a consistent result for both clear sky and all equivalent homogeneous ocean scenes. The uncertainties on the mean differences are relatively small as they are of order 0.04 K and so the larger question concerns uncertainties in any bias terms. Of these, the largest requirement is to reduce the uncertainty in the AATSR spectral filter function because although AATSR is itself radiometrically accurate, the spectral filter function is needed in order to integrate the spectra radiances measured by IASI. This is currently under investigation and it should be possible in future to reduce the filter uncertainty and thus establish whether there

are individual instrument biases or not at the 0.5 K level or smaller.

More generally, the methods developed in this study show that it is possible to inter-compare satellite radiances or BTs with a high precision, and that the spectrometer-radiometer combination offers additional insights, e.g. the use of high spatial resolution information to characterise the homogeneity of the scene, and identify scenes suitable for provision of the most information on instrument bias. The use of cloud-covered pixels has been shown here to extend the BT range over which comparisons can be performed. Therefore suggestions that highly accurate Fourier transform spectrometers (FTS) could be flown in future to inter-calibrate satellite sensors, e.g. Anderson et al. (2004) and the Climate Absolute Radiance and Refractivity Observatory (CLARREO) mission, has some provenance. At the same time, it is also clear from this study that a very good overlap in time is required between the instruments to be inter-compared, and that there is a very tight requirement on knowledge of the spectral filter function for satellite radiometers.

It was only possible to perform a limited study in this work but this has been sufficient to identify the chief aspects which are important for radiometric intercomparisons for climate purposes. A clear challenge for the future is to improve knowledge of the biases, so that careful use may be made of IASI integrated radiances for climate applications. First the analyses should be extended to a longer time series of data on an operational basis. Secondly, extension of the analyses to warmer temperatures, e.g. over land, would be interesting and would extend the temperature range over which the data could be used for climate applications with confidence. Finally, refinement of the AATSR spectral filter function will hopefully permit a tighter error constraint on the quality of the IASI data and hence further assessment of the climate quality of the radiances.

Acknowledgements. IASI has been developed and built under the responsibility of the Centre National d'Etudes Spatiales (CNES, France). It is flown onboard the Metop satellites as part of the EUMETSAT Polar System. The IASI L1 data are received through the EUMETCast near real time data distribution service.

IASI Validation

S. Illingworth et al.

Title Page

Abstract

Introduction

Conclusions

References

Tables

Figures

◀

▶

◀

▶

Back

Close

Full Screen / Esc

Printer-friendly Version

Interactive Discussion



The authors would like to thank NERC for funding S.M. Illingworth and R.J. Parker, NEODC/ESA for access to AATSR data, and EUMETSAT for access to the IASI data. SATSCAN-IR is a project selected by EUMETSAT/ESA under the first EPS/Metop RAO.

References

- 5 Anderson, J. G., Dykema, J. A., Goody, R. M., Hu, H., and Kirk-Davidoff, D. B.: Absolute, spectrally-resolved, thermal radiance: A benchmark for climate monitoring from space, *J. Quant. Spectr. Rad. T.*, 85, 367–383, 2004. 8112
- Blumstein, D., Chalon, G., Carlier, T., Buil, C., Hebert, P., Maciaszek, T., Ponce, G., Phulpin, T., Tournier, B., Simeoni, D., Astruc, P., Clauss, A., Kayal, G., and Jegou, R.: IASI instrument: Technical overview and measured performances, in: *Society of Photo-Optical Instrumentation Engineers (SPIE) Conference Series*, edited by: Strojnik, M., 5543, 2004. 8104
- 10 Brindley, H. E., Geer, A. J., and Harries, J. E.: Climate variability and trends in SSU radiances: A comparison of model predictions and satellite observations in the middle stratosphere, *J. Clim.*, 12, 3197–3219, 1999. 8103
- 15 Camy-Peyret, C. and Eyre, J.: IASI Science Plan, Tech. rep., ISSWG, 1998. 8108
- Clerbaux, C., Hadji-Lazaro, J., Turquety, S., George, M., Coheur, P., Hurtmans, D., Wespes, C., Herbin, H., Blumstein, D., Tourniers, B., and Phulpin, T.: The IASI/MetOp1 Mission: First observations and highlights of its potential contribution to GMES2, *Space Research Today*, 168, 19–24, 2007. 8104
- 20 CNES: IASI CNES, <http://smc.cnes.fr/IASI/>, 2008. 8104
- Dingirard, M. and Slater, P. N.: Calibration of space-multispectral imaging sensors: A review, *Remote Sens. Environ.*, 68, 194–205, 1999. 8106
- ESA: AATSR: Product Handbook, <http://www.leos.le.ac.uk/aatsr/whatis/handbook.html>, 2008. 8105, 8107, 8116
- 25 Harries, J. E., Brindley, H. E., Sagoo, P. J., and Bantges, R. J.: Increases in greenhouse forcing inferred from the outgoing longwave radiation spectra of the Earth in 1970 and 1997, *Nature*, 410, 355–357, 2001. 8103
- Haskins, R., Goody, R., and Chen, L.: Radiance covariance and climate models, *J. Clim.*, 12, 1409–1422, 1999. 8103
- 30 Huang, Y., Ramaswamy, V., Huang, X., Fu, Q., and Bardeen, C.: A strict test in climate modeling

IASI Validation

S. Illingworth et al.

Title Page

Abstract

Introduction

Conclusions

References

Tables

Figures

◀

▶

◀

▶

Back

Close

Full Screen / Esc

Printer-friendly Version

Interactive Discussion



- with spectrally resolved radiances: GCM simulation versus AIRS observations, *Geophys. Res. Lett.*, 34, 2007. 8103
- Llewellyn-Jones, D., Edwards, M. C., Mutlow, C. T., Birks, A. R., Barton, I. J., and Tait, H.: AATSR: Global-change and surface-temperature measurements from ENVISAT, *ESA Bulletin*, 105, 11–21, 2001. 8105
- 5 Mason, I. M., Sheather, P. H., Bowles, J. A., and Davies, G.: Blackbody calibration sources of high accuracy for a spaceborne infrared instrument: The along track scanning radiometer, *Appl. Opt.*, 35, 629–639, 1996. 8105
- Merchant, C. J., Simpson, J. J., and Harris, A. R.: A cross-calibration of GMS-5 thermal channels against ATSR-2, *Remote Sens. Environ.*, 84, 268–282, 2003. 8106, 8108
- 10 Mutlow, C. T., Zavody, A. M., Barton, I. J., and Llewellyn-Jones, D. T.: Sea surface temperature measurements by the along-track scanning radiometer on the ERS 1 satellite: early results, *J. Geophys. Res.*, 99, 22575–22588, 1994. 8105
- Phulpin, T., Blumstein, D., Prel, F., Tournier, B., Prunet, P., and Schlusser, P.: Applications of IASI on MetOp-A: First results and illustration of potential use for meteorology, climate monitoring and atmospheric chemistry, in: *Society of Photo-Optical Instrumentation Engineers (SPIE) Conference Series*, edited by Goldberg, M. D., Bloom, H. J., Huang, A. H., and Ardanuy, P. E., 6684, 66840F.1–66840F.12, 2007. 8104
- 15 of IASI on MetOp-A: First results and illustration of potential use for meteorology, climate monitoring and atmospheric chemistry, in: *Society of Photo-Optical Instrumentation Engineers (SPIE) Conference Series*, edited by Goldberg, M. D., Bloom, H. J., Huang, A. H., and Ardanuy, P. E., 6684, 66840F.1–66840F.12, 2007. 8104
- Qu, J. J., Hao, X., Hauss, B., Wang, C., and Privette, J.: A new approach for radiometric cross calibration of satellite-borne radiometers, in: *Geoscience and Remote Sensing Symposium, 2005. IGARSS '05. Proceedings. 2005 IEEE International*, 6, 4142–4145, 2005. 8107
- 20 Smith, D. L., Delderfield, J., Drummond, D., Edwards, T., Mutlow, C. T., Read, P. D., and Toplis, G. M.: Calibration of the AATSR instrument, *Adv. Space Res.*, 28, 31–39, 2001. 8105
- Wang, L. and Cao, C.: Radiance comparison of IASI and AVHRR on MetOp-A, in: *Society of Photo-Optical Instrumentation Engineers (SPIE) Conference Series*, vol. 6684 of Presented at the Society of Photo-Optical Instrumentation Engineers (SPIE) Conference/, 2007. 8107
- 25 Zavody, A. M., Mutlow, C. T., and Llewellyn-Jones, D. T.: Cloud clearing over the ocean in the processing of data from the along-track scanning radiometer (ATSR), *J. Atmos. Ocean. Tech.*, 17, 595–615, 2000. 8109

IASI Validation

S. Illingworth et al.

[Title Page](#)[Abstract](#)[Introduction](#)[Conclusions](#)[References](#)[Tables](#)[Figures](#)[◀](#)[▶](#)[◀](#)[▶](#)[Back](#)[Close](#)[Full Screen / Esc](#)[Printer-friendly Version](#)[Interactive Discussion](#)

IASI Validation

S. Illingworth et al.

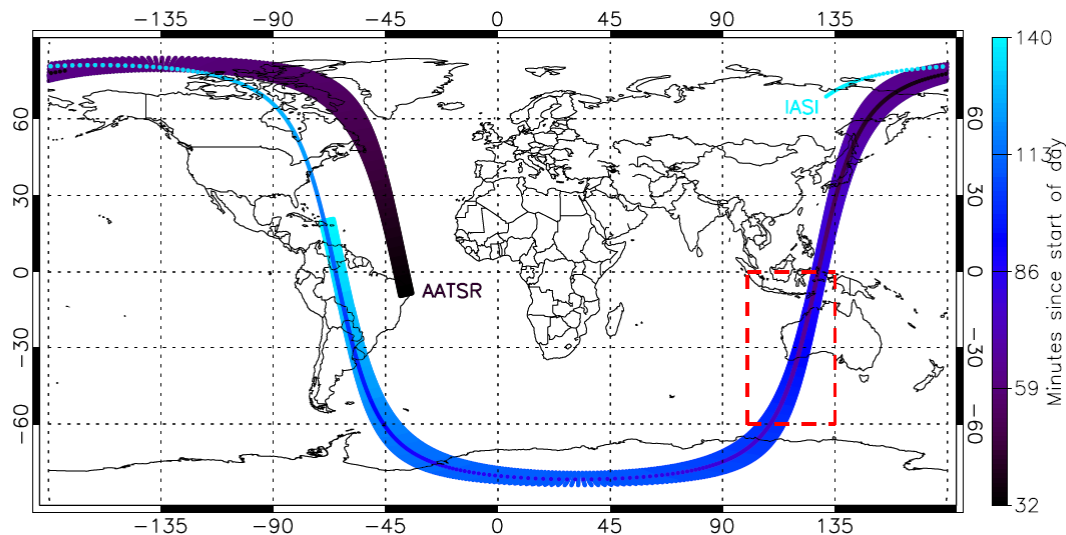


Fig. 1. The time since 00:00 on 01/09/2007 that the IASI and AATSR measurements were made. The first full AATSR swath of the day is shown, along with the first central scan-line of the IASI instrument; the start-time of the IASI and AATSR swaths being 00:35:55 and 00:32:18 respectively. The red-box indicates an area that was selected for cross-calibration, chosen because of the similar temporal values and spatial coincidence between the two instruments.

[Title Page](#)[Abstract](#)[Introduction](#)[Conclusions](#)[References](#)[Tables](#)[Figures](#)[◀](#)[▶](#)[◀](#)[▶](#)[Back](#)[Close](#)[Full Screen / Esc](#)[Printer-friendly Version](#)[Interactive Discussion](#)

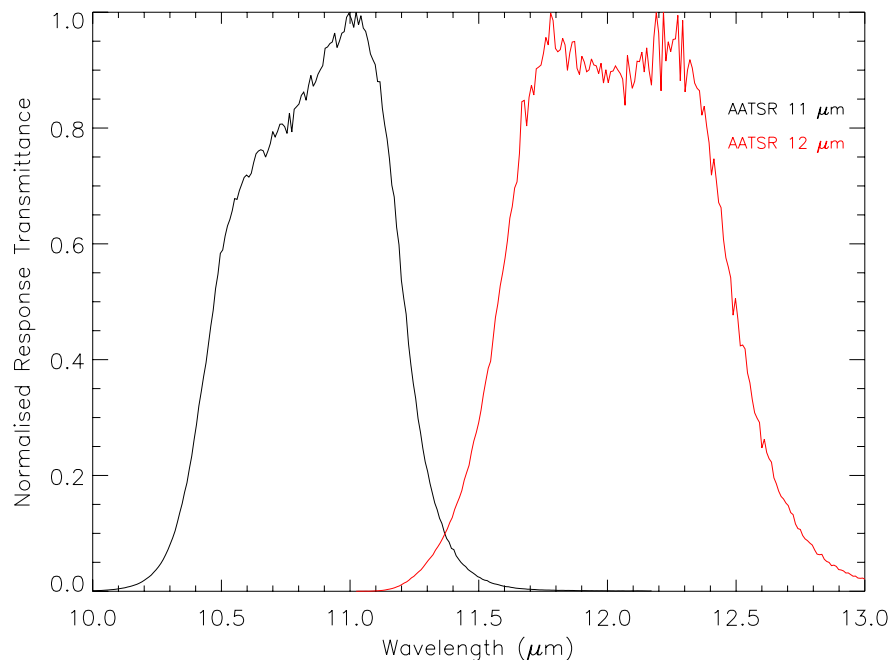


Fig. 2. Spectral filter functions for the 11 μm and 12 μm channels for the Advanced Along-Track Scanning Radiometer (AATSR) on Envisat (ESA, 2008).

[Title Page](#)[Abstract](#)[Introduction](#)[Conclusions](#)[References](#)[Tables](#)[Figures](#)[◀](#)[▶](#)[◀](#)[▶](#)[Back](#)[Close](#)[Full Screen / Esc](#)[Printer-friendly Version](#)[Interactive Discussion](#)

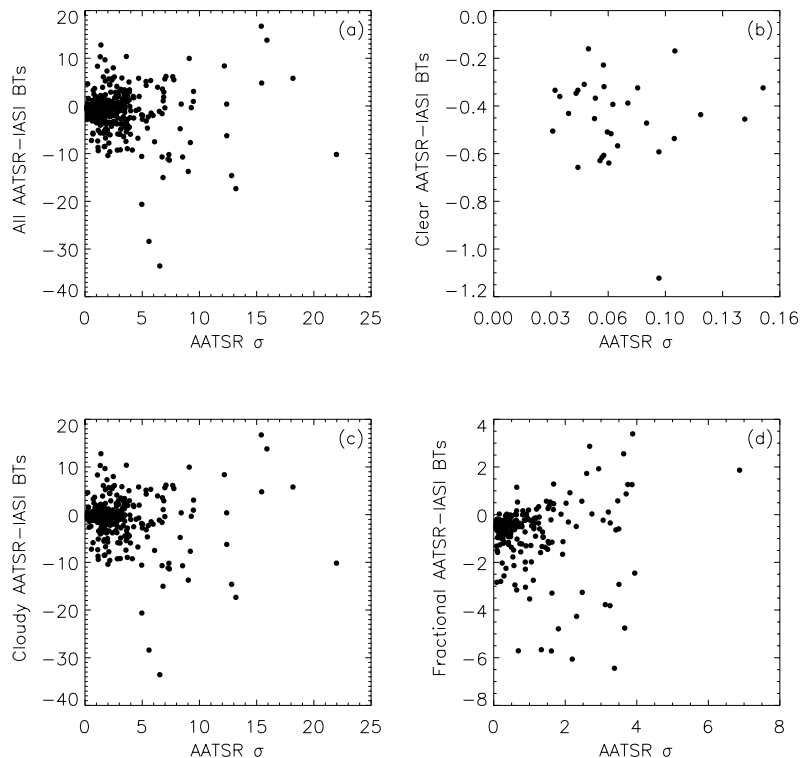


Fig. 3. Comparison of $11\ \mu\text{m}$ IASI equivalent BTs minus mean AATSR BTs in each IASI pixel versus the standard deviation of the AATSR BTs in each pixel: **(a)** all pixels; **(b)** clear sky pixels; **(c)** cloudy (all pixels); **(d)** fractionally cloudy. All match-ups have been selected over the oceans. The small spread of AATSR BTs within each IASI pixel under clear sky conditions is clearly shown

[Title Page](#)[Abstract](#)[Introduction](#)[Conclusions](#)[References](#)[Tables](#)[Figures](#)[◀](#)[▶](#)[◀](#)[▶](#)[Back](#)[Close](#)[Full Screen / Esc](#)[Printer-friendly Version](#)[Interactive Discussion](#)

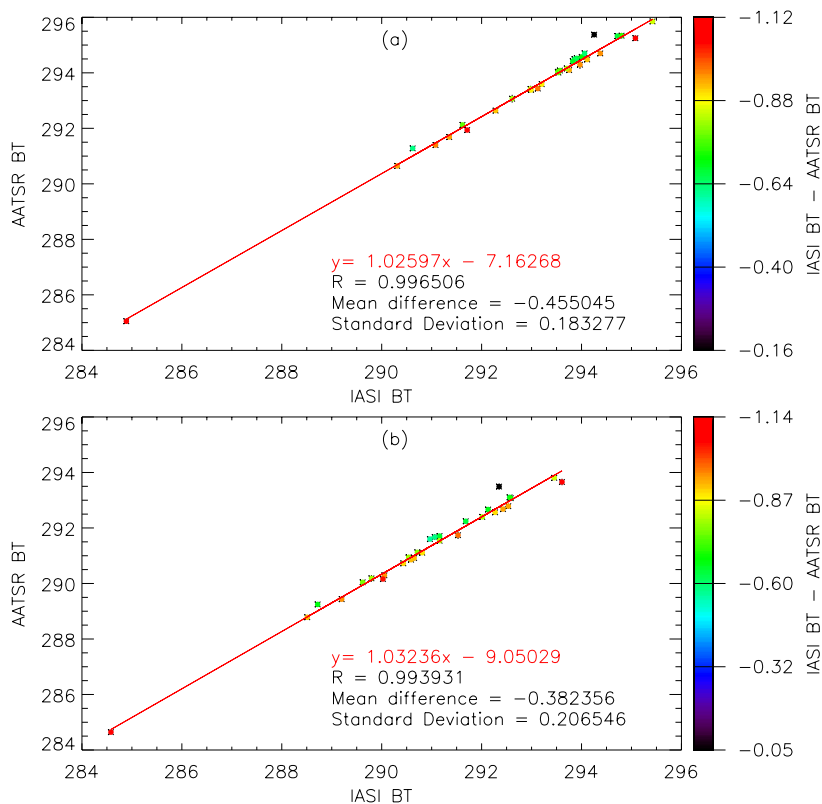


Fig. 4. Comparison of 11 μm and 12 μm IASI equivalent BTs minus mean AATSR BTs in each IASI pixel: **(a)** 11 μm ; **(b)** 12 μm . All match-ups have been selected over the oceans and represent clear sky conditions.

[Title Page](#)[Abstract](#)[Introduction](#)[Conclusions](#)[References](#)[Tables](#)[Figures](#)[◀](#)[▶](#)[◀](#)[▶](#)[Back](#)[Close](#)[Full Screen / Esc](#)[Printer-friendly Version](#)[Interactive Discussion](#)

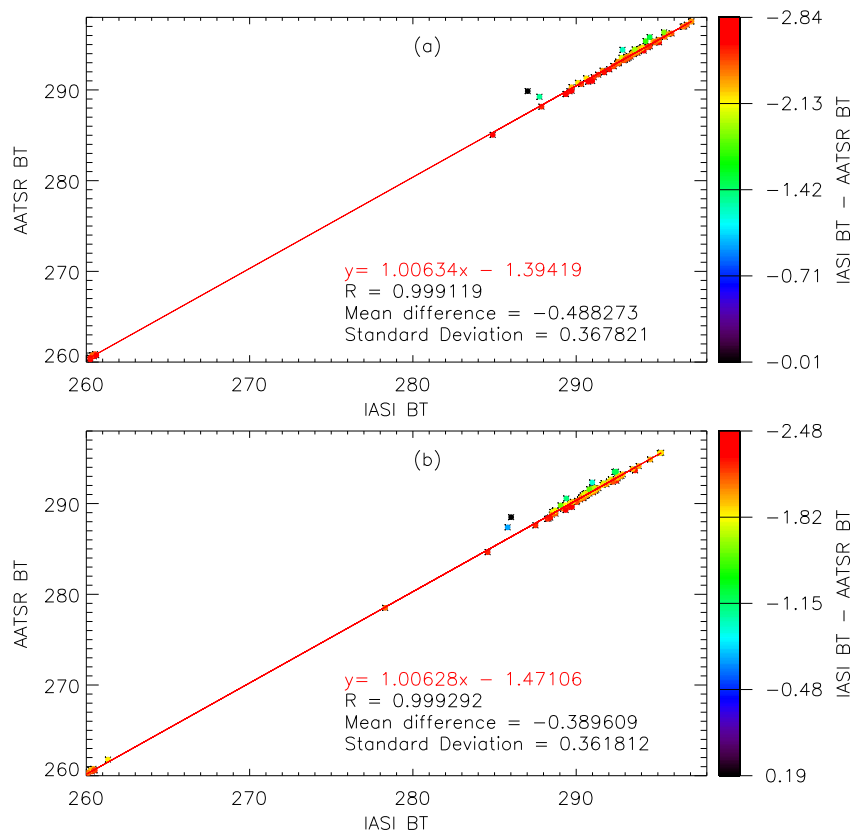


Fig. 5. Comparison of 11 μm and 12 μm IASI equivalent BTs minus mean AATSR BTs in each IASI pixel: **(a)** 11 μm ; **(b)** 12 μm . All match-ups have been selected over the oceans and represent homogenous conditions, where the AATSR BT standard deviation is less than 0.16 K (the clear sky maximum standard deviation).

[Title Page](#)[Abstract](#)[Introduction](#)[Conclusions](#)[References](#)[Tables](#)[Figures](#)[◀](#)[▶](#)[◀](#)[▶](#)[Back](#)[Close](#)[Full Screen / Esc](#)[Printer-friendly Version](#)[Interactive Discussion](#)